IEEE Photonics Journal
An IEEE Photonics Society Publication

Open Access

Optimized Silicon QPSK Modulator With 64-Gb/s Modulation Speed

Volume 7, Number 3, June 2015

Haike Zhu
Linjie Zhou, Member, IEEE
Tao Wang
Lei Liu
Chiyan Wong
Yanyang Zhou
Rui Yang
Xinwan Li, Senior Member, IEEE
Jianping Chen

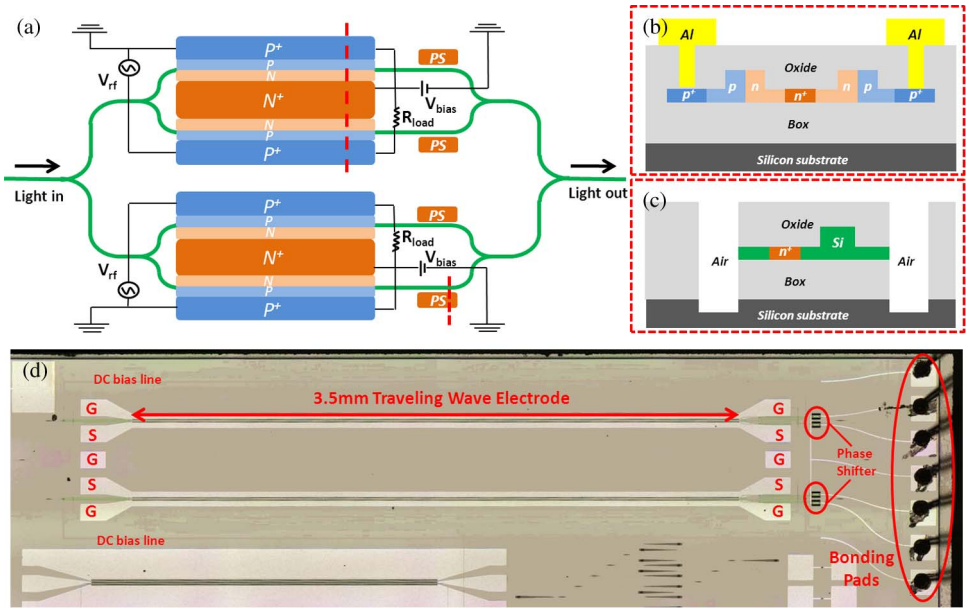

DOI: 10.1109/JPHOT.2015.2425875

Optimized Silicon QPSK Modulator With 64-Gb/s Modulation Speed

Haike Zhu,[1] Linjie Zhou,[1] *Member, IEEE*, Tao Wang,[2] Lei Liu,[2] Chiyan Wong,[2] Yanyang Zhou,[1] Rui Yang,[1] Xinwan Li,[1] *Senior Member, IEEE*, and Jianping Chen[1]

[1]State Key Laboratory of Advanced Optical Communication Systems and Networks, Department of Electronic Engineering, Shanghai Jiao Tong University, Shanghai 200240, China
[2]Transmission Technology Research Department, Huawei Technologies Company Ltd., Shenzhen 518129, China

DOI: 10.1109/JPHOT.2015.2425875

Manuscript received February 3, 2015; revised April 18, 2015; accepted April 20, 2015. Date of publication April 28, 2015; date of current version May 15, 2015. This work was supported in part by the 973 Program under Grant ID2011CB301700, by the 863 Program under Grant 2013AA014402, by the National Natural Science Foundation of China under Grant 61422508, and by the SRFDP of MOE under Grant 20130073130005. Corresponding author: L. Zhou (e-mail: ljzhou@sjtu.edu.cn).

Abstract: We demonstrate a compact silicon quadrature phase-shift keying (QPSK) modulator consisting of two nested Mach–Zehnder interferometers with a size of 4.5-mm^2. The $V_\Pi \cdot L$ of the modulator is 1.4 V $\cdot$ cm with an insertion loss of 8 dB. In addition, 64-Gb/s QPSK modulation is achieved with an error vector magnitude (EVM) of 24.4% and bit error rate (BER) of 2.1×10^{-5} at the received optical power of -10 dBm after the device and an EVM of 31.7% and BER of 8.4×10^{-4} at the received optical power of 0 dBm after 10-km single-mode fiber transmission. The estimated power consumption is 7.1 pJ/bit for the 64-Gb/s QPSK modulation.

Index Terms: Silicon photonics, integrated optical devices, high-speed silicon quadrature phase-shift keying (QPSK) modulator, coherent communication.

1. Introduction

Silicon photonics offers the key merits of small footprint, agile functionalities, and compatibility with integrated microelectronic circuits. Photonic devices based on silicon-on-insulator material have been developing very fast these years with its vast applications in optical communications and interconnects [1]–[4]. As a key component for signal conversion from electrical to optical domain, silicon modulators have always been the research highlight. Recently, 70 Gb/s on–off keying (OOK) optical modulation has been realized on silicon platform by optimizing the traveling wave electrode (TWE) and the interleaved p-n junctions [5]. The next generation optical networks require a high channel data rate of 100 Gb/s, due to the rapid expansion of communication capacity. Advanced modulation formats will be employed due to their high spectral efficiency. The quadrature amplitude modulation (QAM) or the polarization-division-multiplexed quadrature phase-shift keying (PDM-QPSK) together with coherent detection and digital signal processing [6], [7] have been proved to be efficient solutions to improve the bandwidth in long-haul communications for their high receiving sensitivity. As the inherent nonlinearity is present in the *p–n* junction [8], the multi-level signal based silicon QAM modulators have relatively high bit-error-rate (BER) at high modulation speed [9], [10]. On the other hand, the double-level

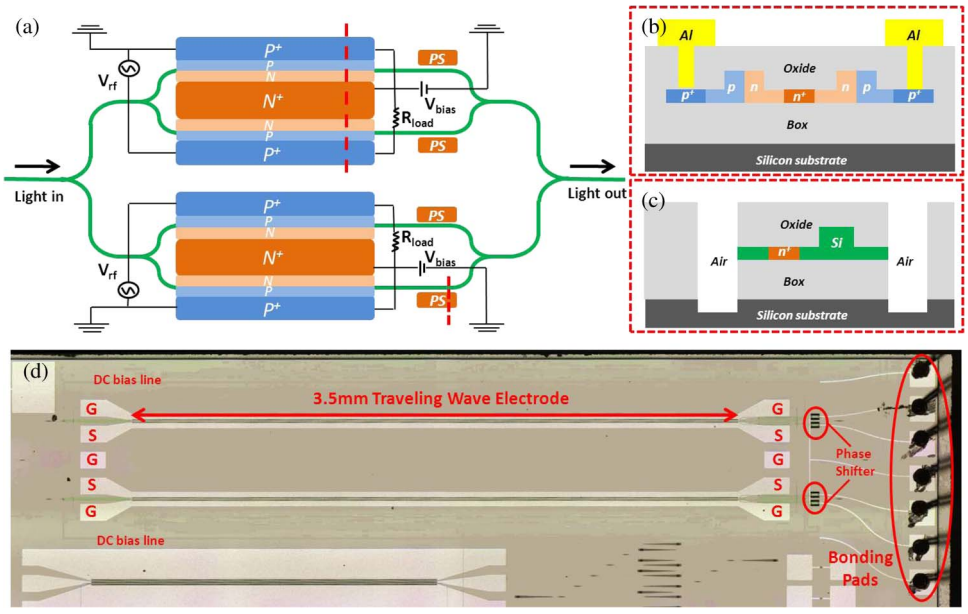

Fig. 1. (a) Device structure of the QPSK modulator. PS: phase shifter. (b) Cross sectional view of the single-drive push-pull TWE. (c) Cross sectional view of the thermo-optic phase shifter. (d) Optical image of the silicon QPSK modulator.

signal based silicon QPSK modulator possesses much higher baud rate with low BER, even though its spectral efficiency is lower than the QAM modulation. Previous work has reported 50 Gb/s QPSK modulation [11]. More recently, 64 Gb/s silicon QPSK and 128 Gb/s silicon PDM-QPSK modulators have been realized based on nested Mach–Zehnder modulators (MZMs) using dual-drive push-pull TWEs [12], [13], demonstrating their suitability for next generation optical coherent communications.

In this paper, we report a 64 Gb/s silicon QPSK modulator with single-drive push-pull TWE. The single-drive push-pull TWE can improve the data quality at a high modulation speed, as the loaded capacitance of the TWE is reduced to half compared to the regular dual-drive push-pull TWE [14]. The modulator can be more compact due to the single-drive design and the number of RF ports is also reduced by half, facilitating high speed electrical package. Compared to the previous demonstration, we use only four thermo-optic phase shifters to set the biases while others use six, making our device more compact. The footprint of our device is 5 mm $\times$ 0.9 mm, which is more than 50% smaller than the prior works based on reverse *p*–*n* junctions. The *p*–*n* junction profile and TWE are carefully optimized to provide higher modulation efficiency at a high modulation speed, leading to reduced RF and DC voltages.

2. Device Structure

Fig. 1(a) shows the structure of the QPSK modulator consisting of two nested MZMs. Each MZM contains a 3.5 mm long single-drive push-pull TWE and two 50 μm long thermo-optic phase shifters. The optical power splitters/combiners in the MZMs are implemented by 1 $\times$ 2 and 2 $\times$ 1 multimode interference (MMI) couplers. Fig. 1(b) shows the cross-sectional view of one MZM. The waveguide dimension is 500 nm $\times$ 220 nm with a slab height of 70 nm. Lateral *p*–*n* junctions are embedded in the MZM arms and have a 100 nm offset towards the *n* doping region. The doping concentrations are 4×10^{17} cm^{-3} and 1×10^{18} cm^{-3} for the *p* and *n* doping regions, respectively. The heavily p^+ doping regions ($\sim 10^{20}$ cm^{-3}) are placed at the outer sides of the Mach–Zehnder interferometer (MZI), and connected to the signal (S) and ground (G) electrodes of the TWE. All the G pads were connected together. The heavily n^+ doping regions ($\sim 10^{20}$ cm^{-3}) are placed in between the MZI arms and connected to the DC bias electrode. The

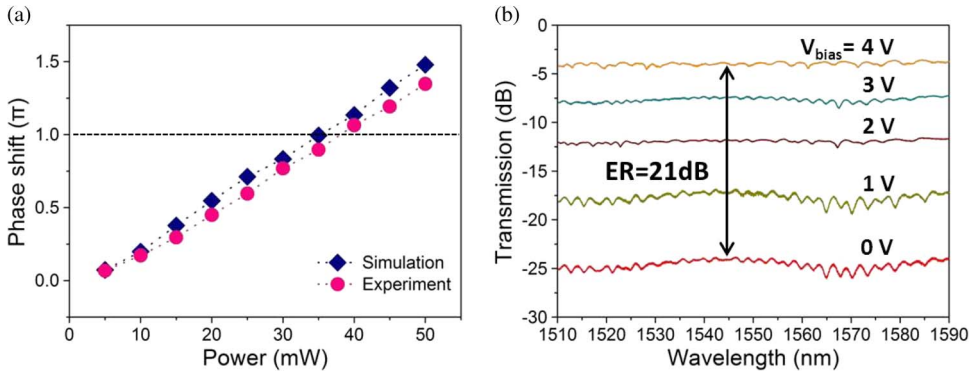

Fig. 2. (a) Simulated and measured thermal phase shift versus applied power. (b) Transmission spectra at various reverse biases.

p^+ and n^+ doping regions are 0.5 μm off the waveguide. Fig. 1(c) shows the cross-sectional view of the thermo-optic phase shifter. It is formed by the heavily n^+ doped silicon slab separated from the waveguide by 0.8 μm to avoid free carrier absorption loss. Deep air trenches surround phase shifters to improve thermal tuning efficiency and meanwhile reduce thermal crosstalk. The fabrication was done using the IME standard CMOS process [15]. Fig. 1(d) shows the optical image of the fabricated device after wire bonding. The DC biases and thermo-optic phase shifters were connected to a printed circuit board (PCB) through wire bonding.

3. Simulation and Experimental Results

We first studied the static characterization of the device. We simulated the temperature change in the thermo-optic phase shifter under various power levels by using COMSOL. The refraction index variation and phase shift were obtained consequently. Fig. 2(a) shows the phase shift changing almost linearly with thermal power consumption, and Π-phase shift is achieved with less than 40 mW power. We tested the thermo-optic phase shifter in a MZI, similar with our previous work [16], and converted the measured result into phase changes as also shown in Fig. 2(a). We find that the phase shift is a little smaller than simulation results, but also has a linear response to thermal power. The Π-phase shift was achieved with less than 40 mW power, which is consistent with simulation.

We then characterized the modulation efficiency of the TWE. Light was coupled into and out of the modulator using lensed fibers. The input light from a tunable laser scanning from 1510 nm to 1590 nm was transverse-electrically (TE) polarized by using a polarization controller. The minimum transmission was obtained by adjusting the four thermo-optic phase shifters. One arm of one nested MZM was biased while the transmission spectrum was measured as shown in Fig. 2(b). The maximum transmission was obtained at 4 V, indicating the Π-phase shift voltage $V_\Pi \approx 4$ V, and therefore, $V_\Pi \cdot L$ is around 1.4 V $\cdot$ cm. We can also find that the static extinction ratio (ER) of the MZM is about 21 dB.

We next measured the small signal response of the electrodes by using a vector network analyzer (VNA) at the DC bias of 3 V. Port 1 and Port 2 of the VNA was connected to one GSGSG probe, while Port 3 and Port 4 was connected to another GSGSG probe. The S_{11} and S_{22} curves, as shown in Fig. 3(a), represent the RF signal return losses at the two TWEs. Both of the responses are below -10 dB over the 50 GHz bandwidth, indicating small signal reflection of the TWE. The S_{31} and S_{42} curves, also shown in Fig. 3(a), represent the RF signal transmission losses of the two TWEs. The electro-electro (EE) 6-dB responses of both TWEs are around 23 GHz. Fig. 3(b) and (c) show the real and imaginary parts of the TWE characteristic impedance, respectively. Return loss becomes low when the impedance approaches 50 Ω, as expected.

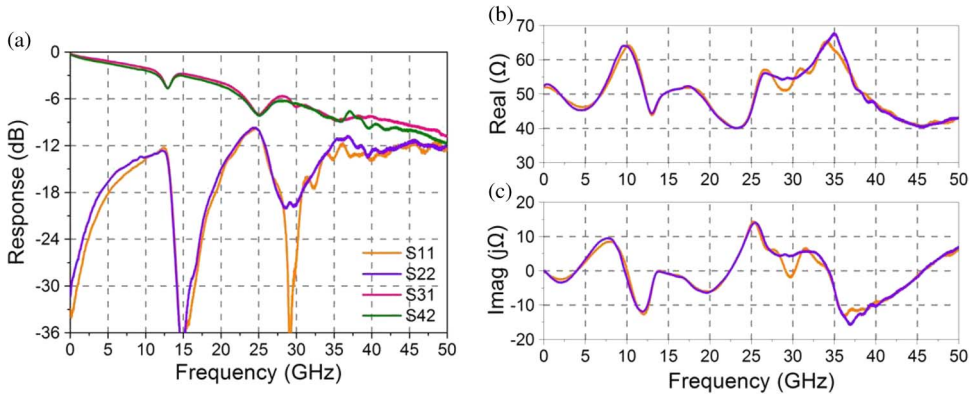

Fig. 3. (a) Electrode EE small signal responses of the two TWEs. (b) and (c) Characteristic impedance of the two TWEs as a function of frequency. (b) Real part and (c) imaginary part.

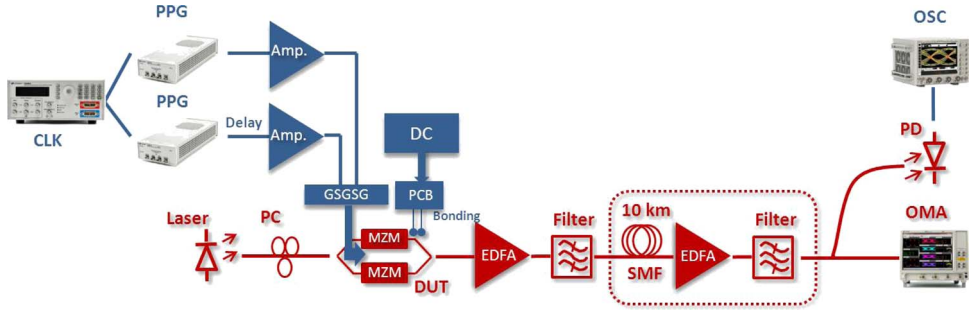

Fig. 4. (a) Experiment setup for high speed modulation measurement. CLK: clock; PPG: pulse pattern generator; Amp: RF amplifier; PCB: printed circuit board; OSC: oscilloscope; PC: polarization controller; DUT: device under test; OMA: optical modulation analyzer.

We then characterized the high-speed performance of the modulator. Fig. 4 shows the experimental setup. A pseudo-random binary sequence (PRBS) signal with a length of $2^{23} - 1$ generated by a pulse pattern generator (PPG) was used as the in-phase (I) drive signal. Another PRBS signal triggered by the same clock is used as the quadrature (Q) drive signal. These two RF signals were amplified to a peak-to-peak voltage of 6 V before being fed into the TWEs via a 40 GHz GSGSG microwave probe. The other ends of the TWEs were terminated with two external 50-ohm resistors via another GSGSG microwave probe. The modulated optical signal from the QPSK modulator was amplified by an erbium-doped optical fiber amplifier (EDFA) to compensate for the modulator insertion loss (IL) and followed by a 1-nm bandwidth optical filter to suppress the ASE noise. The amplified optical signal was either connected to a 50 GHz optical oscilloscope for eye diagram measurement or to an optical modulation analyzer (OMA) for decoding and constellation diagram measurement. Alternatively, a 10 km single mode fiber (SMF), together with an EDFA and a filter, was inserted before the oscilloscope and OMA, as shown in the dashed box of Fig. 4. The input light wavelength was fixed at 1550 nm. In order to generate QPSK signals, the four thermo-optic phase shifters were set to 0, Π, 0.5Π and 1.5Π phases, respectively. The DC biases for both I and Q branches were set at 3 V.

The measured on-chip insertion loss of the modulator was $\sim$8 dB, including $\sim$1 dB loss from MMI couplers and $\sim$7 dB from active waveguides. Fig. 5 shows the measurement results immediately after device and also after 10 km fiber transmission at a bit rate of 64 Gb/s. The three transition levels can be discerned for both QPSK eye diagrams with increased noise after fiber transmission. The optical spectra were record in a 50 GHz frequency span limited by the OMA. The carrier is suppressed in the spectra, exhibiting the QPSK signal characteristics. The

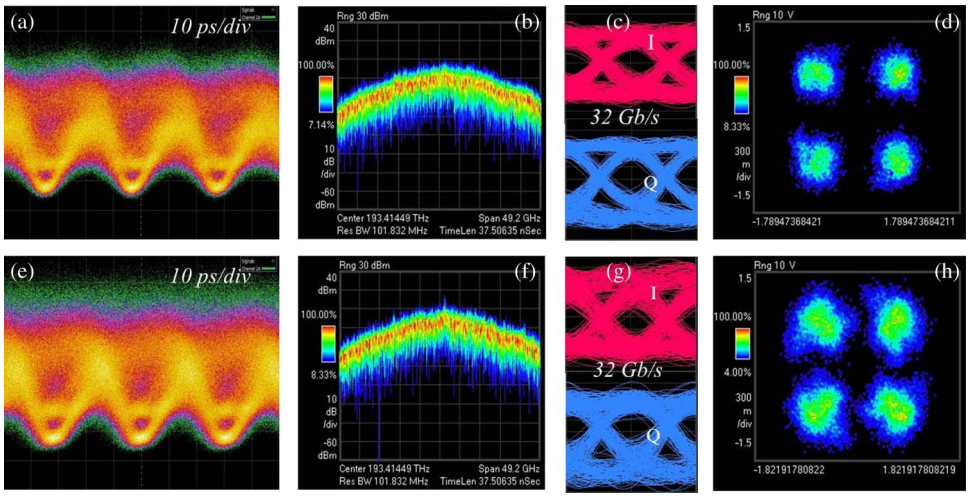

Fig. 5. Measurement results of the 64 Gb/s QPSK modulator after (a)–(d) device and (e)–(h) 10 km transmission in a single mode fiber. (a) and (e) Eye diagrams; (b) and (f) optical power spectra; (c) and (g) decoded in-phase and quadrature eye diagrams; (d) and (h) constellation diagrams.

TABLE I
SILICON (PDM-)QPSK MODULATOR COMPARISON

Ref.	Speed (Gbaud)	$V_\pi \cdot L$ (V·cm)	BER	IL (dB)	Junction type	Size (mm^2)
[11]	25	4	~5×10^{-6} *	4.2	*p-n*	9.1
[19]	28	<0.2	2×10^{-5} *	>5	SISCAP	~2
[12]	32	2.4	~1×10^{-5} *	2.7	*p-n*	10.15
This work	32	1.4	2.1×10^{-5} **	8	*p-n*	4.5

* At the OSNR of 18 dB
** Estimated from EVM at the received optical power of -10 dBm

decoded 32 Gb/s in-phase (I) and quadrature (Q) eye diagrams reveal Q-factors of 5.9 (I) and 6.1 (Q) after device and 5.1 (I) and 5.4 (Q) after fiber transmission. Clear constellation diagrams of the 64 Gb/s signal were obtained. After device, the QPSK signal magnitude and phase errors were 16.7% and 10.7%, respectively, and the error vector magnitude (EVM) was 24.4%. The BER deduced from the measured EVM [17] was 2.1×10^{-5} at a received optical power of -10 dBm. After 10 km transmission, the magnitude and phase errors were increased to 23.1% and 13.2%, respectively, and the EVM increased to 31.7%. At the received optical power of 0 dBm, the deduced BER increased to 8.4×10^{-4}, below the $\sim 10^{-3}$ required in forward error correction (FEC) techniques [18]. The power consumption on the thermo-optic phase shifter is ~40 mW to achieve Π-phase shift. Thus, the power consumption on the four phase shifters is $P_1 = 0 + 20 + 40 + 60 = 120$ mW. The characteristic impedance of the TWE at 32 GHz is ~54 ohm, as shown in Fig. 3(b). Thus, the power consumption on the TWEs can be estimated as $P_2 = 2 \times 1/4 \times V_{pp}^2/R = \sim 333$ mW $(V_{pp} = 6$ V, $R = 54\ \Omega)$. Therefore, the total power consumption is $P = P_1 + P_2 = 453$ mW, corresponding to 7.1 pJ/bit for the 64 Gb/s QPSK modulation.

Finally, we compared our device with previous all-silicon (PDM-) QPSK modulators [11], [12], [19], as shown in Table 1. Our device possesses the highest modulation efficiency of 1.4 V · cm and smallest device size of 4.5 mm^2 among the devices based on reverse *p–n* junctions, but at the price of high chip insertion loss of 8 dB. The device based on SISCAP has the lowest $V_\Pi \cdot L$ of all modulators, benefiting from the high modulation efficiency of the capacitor structure, but

the fabrication is relatively complicated. Note that a 56 Gbaud all-silicon QPSK modulator had recently been reported [20]. However, the device has a high on-chip insertion loss of 34 dB, mainly caused by the long active waveguide and optical equalizer.

4. Conclusion

We have demonstrated a high-speed QPSK modulator on the silicon platform. Measurements show that our 64 Gb/s QPSK modulator has an EVM of 24.4% and a BER of 2.1×10^{-5} at a received optical power of -10 dBm after device and an EVM of 31.7% and a BER of 8.4×10^{-4} at the received optical power of 0 dBm after 10 km SMF transmission. The modulator has low power consumption of 7.1 pJ/bit. Given its compact size and simplified RF interface, the QPSK modulator can be employed to build high-speed transmitters for optical communications and interconnects.

References

[1] B. Jalali and S. Fathpour, "Silicon Photonics," *J. Lightw. Technol.*, vol. 24, pp. 4600–4615, Dec. 2006.
[2] D. Miller, "Device requirements for optical interconnects to silicon chips," *Proc. IEEE*, vol. 97, no. 7, pp. 1166–1185, Jul. 2009.
[3] G. T. Reed, G. Mashanovich, F. Y. Gardes, and D. J. Thomson, "Silicon optical modulators," *Nat. Photon.*, vol. 4, pp. 518–526, Aug. 2010.
[4] P. Dong, Y.-K. Chen, G.-H. Duan, and D. T. Neilson, "Silicon photonic devices and integrated circuits," *Nanophoton.*, vol. 3, no. 4/5, pp. 215–228, Mar. 2014.
[5] H. Xu *et al.,* "High-speed silicon modulator with band equalization," *Opt. Lett.*, vol. 39, no. 16, pp. 4839–4842, Aug. 2014.
[6] C. R. S. Fludger *et al.,* "Coherent equalization and POLMUX-RZ-DQPSK for robust 100-GE transmission," *J. Lightw. Technol.*, vol. 26, no. 1, pp. 64–72, Jan. 2008.
[7] P. J. Winzer, A. H. Gnauck, C. R. Doerr, M. Magarini, and L. L. Buhl, "Spectrally efficient long-haul optical networking using 112-Gb/s polarization-multiplexed 16-QAM," *J. Lightw. Technol.*, vol. 28, no. 4, pp. 547–556, Feb. 2010.
[8] A. Ayazi, T. Baehr-Jones, Y. Liu, A. E. Lim, and M. Hochberg, "Linearity of silicon ring modulators for analog optical links," *Opt. Exp.*, vol. 20, no. 12, pp. 13115–13122, Jun. 2012.
[9] P. Dong *et al.,* "224-Gb/s PDM-16-QAM Modulator and Receiver Based on Silicon Photonic Integrated Circuits," in *Proc. Opt. Fiber Commun. Conf.*, Los Angeles, CA, USA, 2013, pp. 1–3.
[10] T. Li *et al.,* "Demonstration of 6.25 Gbaud advanced modulation formats with subcarrier multiplexed technique on silicon Mach-Zehnder modulator," *Opt. Exp.*, vol. 22, no. 16, pp. 19818–19823, Aug. 2014.
[11] P. Dong, L. Chen, C. Xie, L. L. Buhl, and Y.-K. Chen, "50-Gb/s silicon quadrature phase-shift keying modulator," *Opt. Exp.*, vol. 20, no. 19, pp. 21181–21186, Sep. 2012.
[12] K. Goi *et al.,* "Low-loss high-speed silicon IQ modulator for QPSK/DQPSK in C and L bands," *Opt. Exp.*, vol. 22, no. 9, pp. 10703–10709, May 2014.
[13] K. Goi *et al.,* "128-Gb/s DP-QPSK using low-loss monolithic silicon IQ modulator integrated with partial-rib polarization rotator," in *Proc. Opt. Fiber Commun. Conf.*, Los Angeles, CA, USA, 2014, pp. 1–3.
[14] P. Dong, L. Chen, and Y. K. Chen, "High-speed low-voltage single-drive push-pull silicon Mach-Zehnder modulators," *Opt. Exp.*, vol. 20, no. 6, pp. 6163–6169, Mar. 2012.
[15] L. Tsung-Yang *et al.,* "Silicon modulators and germanium photodetectors on SOI: Monolithic integration, compatibility, and performance optimization," *IEEE J. Sel. Top. Quant. Electron.*, vol. 16, no. 1, pp. 307–315, Jan./Feb. 2010.
[16] Q. Wu *et al.,* "Silicon thermo-optic variable optical attenuators based on Mach–Zehnder interference structures," *Opt. Commun.*, vol. 341, pp. 69–73, Dec. 2015.
[17] R. Schmogrow *et al.,* "Error vector magnitude as a performance measure for advanced modulation formats," *IEEE Photon. Technol. Lett.*, vol. 24, no. 1, pp. 61–63, Jan. 2012.
[18] F. Chang, K. Onohara, and T. Mizuochi, "Forward error correction for 100 G transport networks," *IEEE Commun. Mag.*, vol. 48, no. 3, pp. S48–S55, Mar. 2010.
[19] B. Milivojevic *et al.,* "112Gb/s DP-QPSK transmission over 2427 km SSMF using small-size silicon photonic IQ modulator and low-power CMOS driver," in *Proc. Opt. Fiber Commun. Conf.*, Los Angeles, CA, USA, 2013, pp. 1–3.
[20] P. Dong *et al.,* "Silicon in-phase/quadrature modulator with on-chip optical equalizer," in *Proc. Eur. Conf. Opt. Commun.*, Cannes, France, 2014, pp. 1–3.